NANO LETTERS

pubs.acs.org/NanoLett

Letter

Enhancement of Amplified Spontaneous Emission by Electric Field in $CsPbBr_3$ Perovskites

Yang Li,* Hang Hu, Ahmed Farag, Thomas Feeney, Isabel Allegro, Uli Lemmer, Ulrich W. Paetzold,* and Ian A. Howard*

Cite This: https://doi.org/10.1021/acs.nanolett.2c02944

Read Online

ACCESS | Metrics & More | Article Recommendations | Supporting Information

ABSTRACT: Perovskite gain materials can sustain continuous-wave lasing at room-temperature. A first step toward the unachieved goal of electrically excited lasing would be an improvement in gain when electrical stimulation is added to the optical. However, to date, electrical stimulation supplementing optical has reduced gain performance. We find that amplified spontaneous emission (ASE) in a $CsPbBr_3$ perovskite light-emitting diode (LED) held under invariant subthreshold optical excitation can be turned on/off by the addition/removal of an electric field. A positive bias voltage leads to a factor of 3 reduction in the optical ASE threshold, the cause of which can be attributed to an enhancement of the radiative rate. The slow components (10 s time scale) of the modulation in the photoluminescence and ASE when the voltage is changed suggest that the relocation of mobile ions trigger the increased radiative rate and observed lowering of ASE thresholds.

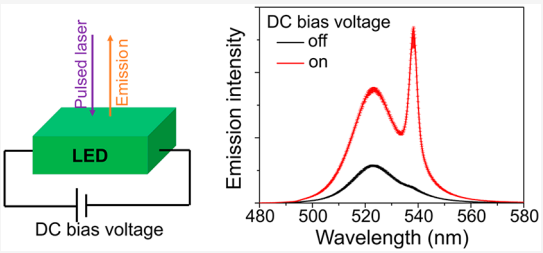

KEYWORDS: *amplified spontaneous emission, perovskite, field enhancement, ion migration*

Halide perovskite semiconductors are an emerging class of laser gain media[1−14] due to their high absorption coefficient, emission color tunability, and low-cost solution processability. Following the milestone of room-temperature continuous-wave (CW) lasing,[14] several efforts[15−20] on intense electrical driving of light-emitting diodes (LEDs) have been made. One of the most exciting results is an external quantum yield of 1% at 10 kA cm^{-2} achieved under nanosecond electrical pulses.[19] This pushes the electrically injected carrier density to almost the same as the threshold carrier density needed for lasing under picosecond optical pulsed excitation.[19] However, electrically pumped lasing is still not realized.

Simultaneous optical and electrical excitation of perovskite gain media is useful to study the transition from optical to electrical lasing. Several studies have been performed on dual optical-electrical excitation,[21−25] and devices with different structures have been explored, i.e., vertical LED structures with[23,25] and without[21] current injection, a horizontal transistor structure,[22] and a metal−insulator−semiconductor structure.[24] These previous results found that electrical stimulation either did not effect or had an adverse effect on amplified spontaneous emission (ASE) and lasing thresholds, even though photoluminescence (PL) enhancement[22,24] upon electrical excitation has been observed (this was attributed to trap filling). In contrast to the above work, we find a reduction (by a factor of 3) in the ASE threshold when a positive voltage over 4 V is applied to $CsPbBr_3$ perovskite LEDs. We demonstrate that optical ASE can be repeatedly switched on/off by modulation of electrical bias. We ascribe the ASE enhancement to an increase in the second-order radiative rate constant and decrease in nonradiative first and second-order rate constants caused by the application of electric field. The slow response of the PL and ASE upon modulation of the bias voltage suggest that mobile ions are responsible for the effect. Ion migration[26−28] has been widely observed in perovskite-based optoelectronic devices. For example, it is the main cause of the well-known hysteresis behavior,[29] and it has been previously suggested that electric-field-assisted motion of the mobile ions under operating conditions can alter the electric field and carrier distribution within solar cells, LEDs, and photodetectors.[30−36]

We first develop perovskite LED devices whose device architecture is tuned to minimize the optically pumped ASE threshold. These employ a smooth $CsPbBr_3$ emissive layer fabricated through the previously reported process of annealing a quasi-2D precursor film at a high temperature.[37,38] The excited-state population in this layer is known to be dominated by free charge carriers, and this is beneficial for its gain performance.[37,38] It is sandwiched between a ZnO electron transporting layer (ETL) and a poly[(9,9-dioctylfluorenyl-2,7-diyl)-*co*-(4,4′-(*N*-(4-sec-butyl-phenyl)diphenylamine) (TFB)

Received: July 26, 2022
Revised: February 1, 2023

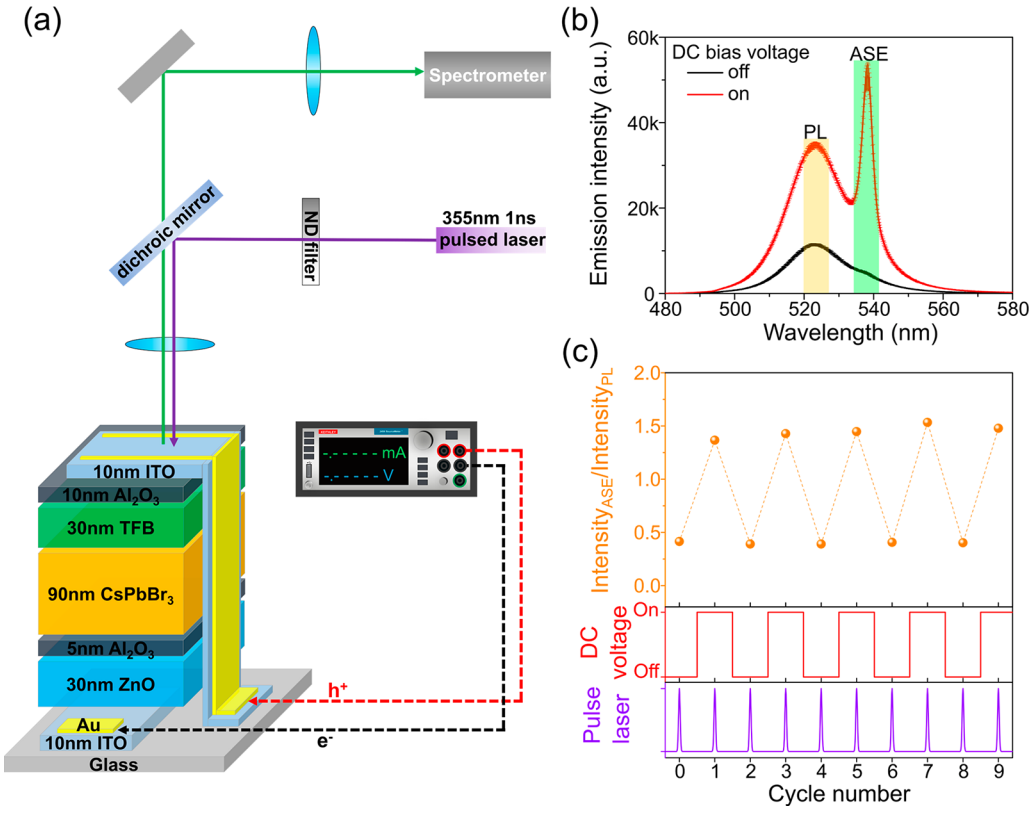

Figure 1. Enhancing optically pumped PL and ASE intensity of perovskite LEDs by application of a positive bias voltage. (a) Schematic of the experimental setup exhibiting the collection of perovskite LED emission under dual excitation of a 355 nm laser (1 ns pulse length, 1 kHz) and a DC bias voltage. The pulsed laser is incident from the HTL side and the measurements are conducted in air. (b) Emission spectra of the perovskite LED acquired using subthreshold optical excitation (~0.8P_{th}) without (black line) and with (red line) a positive bias of 6 V. ASE is essentially absent without applied electrical bias, but clearly visible with electrical bias (although the optical pumping remains identical). Error bar represents the standard deviation calculated from five off/on cycles. (c) Reproducibility of effect illustrated by the ratio of the peak intensity in the "ASE-region" (green area in (b)) relative to the peak intensity in the PL region (orange area in (b)) over several off/on cycles with sufficient time for the ratio to settle. The optical excitation remains at ~0.8P_{th}.

hole transporting layer (HTL). Integrating a $CsPbBr_3$ film into an LED device significantly reduces its ASE performance due to the worse optical confinement in $CsPbBr_3$ layer caused by the change in the dielectric environment (Figure S1a,b). To optimize the ASE performance in an LED structure (opaque device), device engineering was undertaken (Supplementary Note 1 and Figure S1c,d) that resulted in an optimal semitransparent device (Figure 1a) using thin sputtered indium doped tin oxide (ITO) electrodes. To compensate for the thinness of the ITO layers, gold grids (0.2 mm in width) are employed to reduce the series resistance of the LED device. The performance of these devices optimized for low ASE threshold (and their stability) is summarized in Figure S2. Despite the low performance of the LEDs that are unstable at very high (>8 V) voltages needed for significant electroluminescence (EL), they are stable at the sub EL turn-on conditions (≤6 V) used below. The ASE threshold of this LED structure optimized for best optical gain performance is still around two times higher (worse) than that of the pristine $CsPbBr_3$ film (Figure S1) even though the absorption loss due to the electrical contacts and functional layers of the LED has been excluded. This is not an effect of scattering as the $CsPbBr_3$ film in the LED is as smooth (crystal size ~44 nm, Figure S3) as that of the pristine film.[37] Based on such an LED structure optimized for the lowest optically pumped ASE threshold, we report a significant further improvement of the optical ASE threshold upon the application of an electrical bias.

To simultaneously pump the perovskite LED optically and electrically, a 355 nm laser with 1 ns pulse length (1 kHz) was used for optical stimulation alongside a DC bias voltage generated from a Keithley Source Meter Unit. Figure 1a illustrates the experimental setup to record emission spectra with and without the bias voltage. Unless otherwise stated, the pulsed laser is incident from the HTL side of the semi-transparent LED, and the above 355 nm pulsed laser is the only optical source for the dual excitation experiments (conducted in air). Figure 1b shows the drastic change in emission spectra upon switching the 6 V bias voltage (stabilizing for 5 s) on and off while the optical excitation from the pulsed laser is held constant at ~80% of the ASE threshold in the absence of applied bias (0.8P_{th}, P_{th} ~ 600 μJ cm^{-2}). When a bias voltage is applied, the PL is enhanced and the ASE is switched on. This observation is highly reproducible as seen in the small standard deviation of the emission spectra measured over 5 on/off cycles (error bars in Figure 1b), and the almost unchanging ratio between the PL and ASE peaks over subsequent cycles (Figure 1c). Note that the EL of the LED does not contribute to the collected emission because the EL does not turn on yet at 6 V (Figure S2). Therefore, the applied bias must be increasing the emission intensity from the optically generated excited states.

https://doi.org/10.1021/acs.nanolett.2c02944
Nano Lett. XXXX, XXX, XXX−XXX

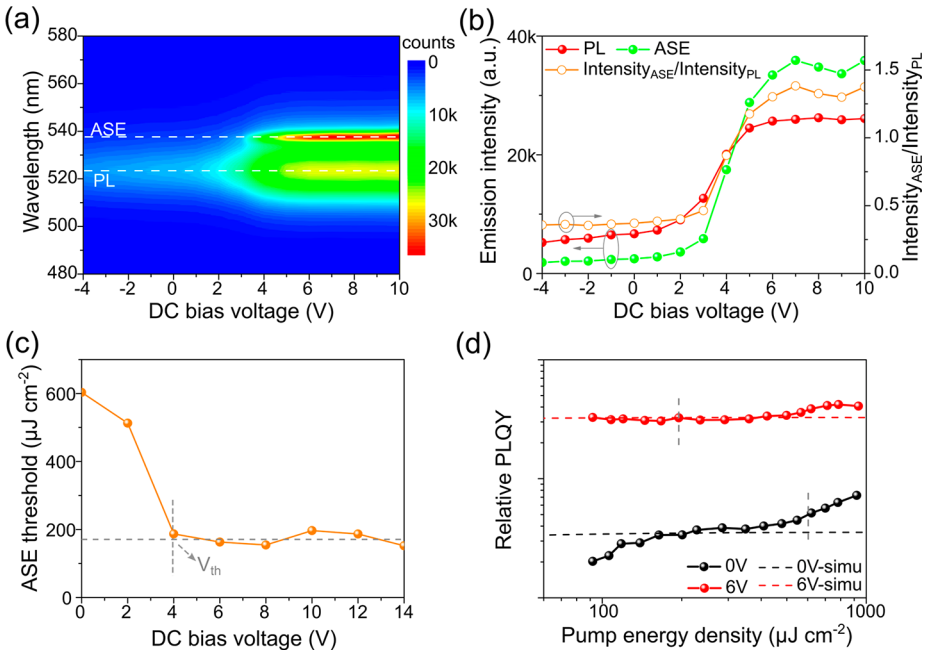

Figure 2. Effect of the bias voltage on PL and ASE enhancement. (a) 2D contour plots of emission spectra versus the DC bias voltage. The laser power is fixed at ~0.8P_{th} (355 nm, 1 ns duration, 1 kHz), and the voltage is scanned in the forward direction with 1 V step and 2 s stabilizing time for each voltage. (b) Plots of the ASE and PL peak intensity and their ratios versus the DC bias voltage. (c) Plots of the ASE thresholds versus the DC bias voltage. All data suggest that no additional improvement in ASE is achieved with further increase in applied bias over 4 V. (d) Relative PLQYs under pulsed laser excitation versus pump energy densities. The relative PLQYs (solid lines) are calculated through dividing the emission integral by excitation energy (shown in Figure S6), and the red/black dashed lines are the simulated PLQYs using the rate equations (shown in Figure S7). The gray dashed lines indicate the corresponding ASE threshold.

To investigate the influence of the bias voltage on the emission of the optically generated states (i.e., PL and ASE intensity), the emission spectra are collected upon scanning the voltage from −4 to 10 V while the pulsed laser power is still held at 0.8P_{th}. Figure 2a shows how the emission spectra change as the bias voltage is slowly increased. Broadband PL (peaked at 523 nm) dominates the emission spectra until 3 V. Further increasing the voltage leads to the emergence of ASE (peaked at 538 nm), which is accompanied by a significant PL enhancement. EL is much weaker than PL so does not contribute to this enhancement (Figure S4). A reduction in PL intensity is visible in the negative bias regime (Figure 2b). In the positive bias regime, ASE intensity, PL intensity, and their ratio all increase with the voltage bias and finally remain almost unchanged (over 6 V). A reverse voltage scan (from 10 V to −4 V with 2 V s^{-1} scan rate, Figure S5) shows significant hysteresis, which often indicates ion migration in perovskite-based devices.[26,29] Through scanning the excitation pulse energy of the laser for a sequence of different bias voltages (Figure S6), the ASE threshold as a function of applied bias is derived, as presented in Figure 2c. The exposure time of the sample to high biases and laser intensities was limited to minimize device degradation (see experimental section of Supporting Information). Increasing the positive bias voltage from 0 to 4 V leads to a significant reduction in ASE threshold from ~600 μJ cm^{-2} to ~200 μJ cm^{-2}. Considering the transmission of the ITO/Al_2O_3/TFB is only 60%, the lowered threshold could be considered to be 120 μJ cm^{-2} for comparison against the reference perovskite on glass with a threshold of 160 μJ cm^{-2} (Figure S1). Clearly, the application of bias significantly improves the ASE performance of the material. Further increasing the voltage above 4 V does not further reduce the ASE threshold (nor increase the PL intensity). As discussed further below, the lack of further change beyond a "threshold" bias is consistent with a spatial rearrangement of mobile ions causing the changes in emission. We note that the redistribution of ions depends on the driving force and time, and in that sense, 4 V is not a real threshold voltage but reflects that the bias was applied only for a limited time (1.0 s). Applying lower voltages for longer times could also lead to sufficient rearrangement.

Before examining why field-induced rearrangement of mobile ions is the most likely explanation for the observations, we first consider how the field affects the photoexcited charge carriers' recombination pathways. The relative PL quantum yield (PLQY) as a function of pulse energy is shown in Figure 2d with and without the 6 V bias. To qualitatively discuss these data, the ABC model for recombination dynamics and PLQY given in eqs 1 and 2 is used.

$$\frac{dn}{dt} = G(t) - k_1 n - (k_{2r} + k_{2nonr})n^2 - k_3 n^3 \quad (1)$$

$$\mathrm{PLQY}(n) = \frac{k_{2r} n}{k_1 + (k_{2r} + k_{2nonr})n + k_3 n^2} \quad (2)$$

where $G(t)$ is the generation rate, k_1 is the trap-assisted recombination coefficient, k_{2r} and k_{2nonr} are radiative and nonradiative second-order rate coefficients, and k_3 is the Auger rate coefficient. The origin of k_{2nonr} is not entirely clear but could be related to a nonradiative process involving two free carriers and a trapped one.[39−44] As discussed below, inclusion of a k_{2nonr} is necessary to understand the observed changes in PLQY with bias. As seen from eq 2, the PLQY will first increase with carrier density until k_1 is negligible compared to $(k_2 + k_{2nonr})n$. The PLQY will then saturate and decrease once

https://doi.org/10.1021/acs.nanolett.2c02944
Nano Lett. XXXX, XXX, XXX−XXX

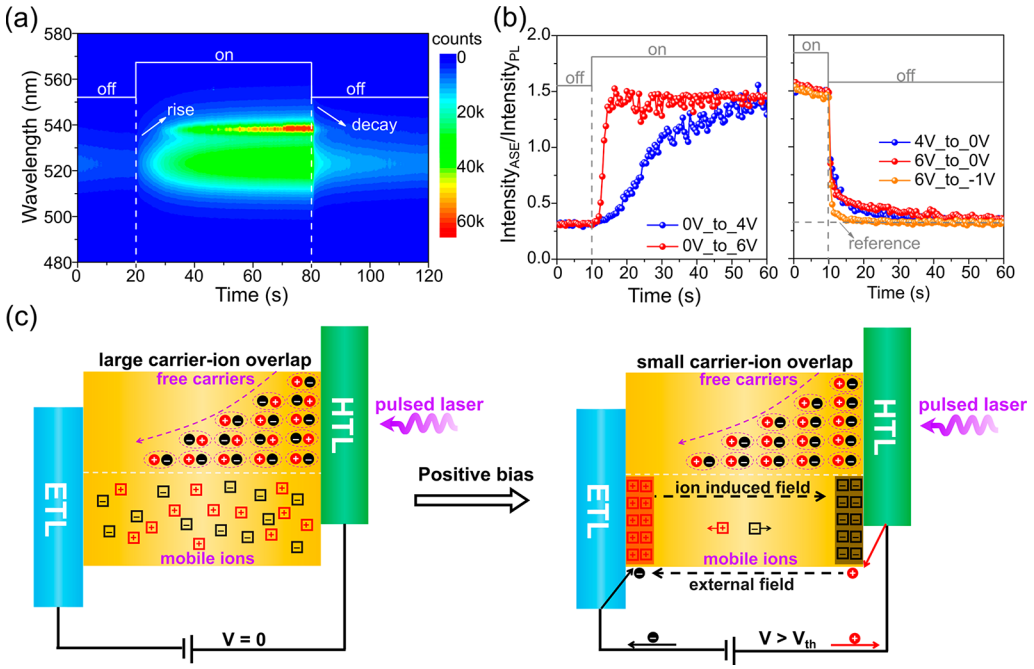

Figure 3. Effect of ion migration on ASE performance. (a) Transient behavior of emission spectra after switching on and off the 4 V bias. (b) Comparison of the ASE rise (left) and decay (right) transients after switching on and off between different bias voltages. The time resolution for the transients is 0.5 s. (c) Schematic illustration of the increased spatial separation of the photogenerated charge carriers and mobile ions due to redistribution of ions to interfaces caused by the applied field. The circle and square symbols in the orange area indicate the free carriers and mobile ions, respectively. The model also shows that the field generated by the redistributed ions opposes that of the external field.

the carrier density becomes so high that k_3n^2 becomes comparable with $(k_2 + k_{2nonr})n$. The PLQY below ASE threshold remains almost constant for both 0 and 6 V data sets (Figure 2d). This indicates that second-order recombination channels dominate, and both first (trap-related) and third-order (Auger) loss processes are negligible in this fluence range. The absence of significant Auger recombination is reasonable considering literature rate constants;[37,45] numerical simulations in Figure S7 indicate that the nanosecond pulses of such fluences generate carrier densities less than 10^{19} cm^{-3} necessary for Auger processes to become competitive. After the ASE threshold, the PLQY increases significantly for the 0 V case, but hardly for the 6 V case. This indicates that the PLQY for the 6 V case was already very high before the ASE threshold and would barely be increased by the faster radiative processes introduced by ASE. This is also consistent with the saturated PLQY values for 6 V data being 8 times higher than for the 0 V data, which indicates that the fraction of second-order radiative recombination, $k_{2r}/(k_{2r} + k_{2nonr})$, has significantly increased after the application of bias. Assuming that the quantum yield is unity for the 6 V data after the ASE threshold, $k_{2r}/(k_{2r} + k_{2nonr})$ before threshold can be estimated as 0.09 and 0.74 for the 0 and 6 V data, respectively. Time-resolved PL (TRPL) studies (Figure S8) confirm that k_1 decreases and $k_{2r} + k_{2nonr}$ increases upon the application of bias. Figure S9 presents how parameters for all the rate constants can be chosen to self-consistently explain the PLQY and TRPL data. In summary, the application of bias is found to decrease k_1 and k_{2nonr}, both pathways associated with traps. An increase in k_{2r}, perhaps due to faster charge motion, is also suggested.

We now turn to look at how the applied bias might lead to these photophysical changes. As a first check, we replace the DC voltage bias with a CW optical bias (Figure S10). The CW optical bias does not alter the ASE threshold at all. This excludes trap filling as the primary cause of PL and ASE enhancement, as if this was the cause then the CW optical excitation should have a similar effect. As a second check, we can be certain that the accelerated second-order process has nothing to do with the increased carrier densities from the electrical injection. This is because the equilibrium carrier density generated from DC bias voltage is less than 1.6×10^{14} cm^{-3} (Supplementary Note 2), which is much lower compared to the photogenerated free carriers (>10^{18} cm^{-3}) by 1 ns pulsed laser. Also, we did not observe light-induced electrical injection as the current density of the LED does not change when the pulsed laser is turned on or off (Figure S11).

To uncover the origin of the bias-assisted enhancement in radiative recombination process, we track the emission spectra on the time scale of seconds upon turning on and off the bias voltage while the optical pump intensity is maintained at ~0.8P_{th}. This is presented in Figure 3a and Figure S12. Note that continuous drive LED (at 6 V) for 1 min only leads to a small temperature rise (<5 °C, Figure S13), and hence the Joule heating induced emission change can be neglected.[46] After switching on the 4 V bias, the emission intensity slowly rises, followed by the emergence of the ASE signature after ~10 s. Similarly, upon switching off the bias voltage, the ASE signature also has a slow component (~10 s) to its decrease (as does the PL). The very slow response of the PL and ASE to the application of field can be slightly accelerated (<5 s) by increasing the bias to a higher positive voltage (4 V vs 6 V) or applying a negative voltage (0 V vs −1 V) when turning off the bias, as shown in Figure 3b. Note that the transients upon switching off the bias also show a fast decay component (Figure 3b right) not present in the buildup. We postulate that the field in the reverse bias direction induced by redistributed ions could assist charge extraction of the photogenerated carriers (this, accompanied by the redistribution of ions back

https://doi.org/10.1021/acs.nanolett.2c02944
Nano Lett. XXXX, XXX, XXX−XXX

into the device could explain the transient reverse currents observed when the bias is returned to zero as shown in Figure S14). Increasing the operating temperature of the LEDs to 65 °C was attempted (Figure S15), but a statistically significant alteration of the rise/decay dynamics of the PL was not observed. However, slow components on the time scale of second clearly remain even at the elevated temperature. The long time scale of the process and the dependence of the transient on the driving force are strong indications that mobile ions play a significant role in causing the change in PL and ASE characteristics upon the application of an electrical bias.[47]

A schematic of the hypothesized voltage-modulated ion migration is presented in Figure 3c to understand the mobile ions' effect on the radiative recombination process and ASE transient behavior. Both positive ions (Cs^+, Pb^{2+}) and negative ions (Br^-) are considered in the schematic, but this discussion is also valid if only one type of mobile ion is present. Considering the material structure and recent studies, Br^- ions are expected to dominate.[26] At short circuit conditions (0 V), the mobile ions will be evenly distributed across the $CsPbBr_3$ film. The ionic defects throughout the bulk could reduce the radiative recombination rate by scattering and trapping,[48] while increasing the trap-related first and second-order nonradiative recombination.[39−44]

If a positive bias voltage is applied, the external field will drift the negative and positive ions toward the $CsPbBr_3$/HTL and $CsPbBr_3$/ETL interfaces, respectively. This would result in a reduced trap density in the bulk region where most of the photogenerated carriers exist. As a consequence, a decrease in the first and second-order trap-associated rates and an increase in the second-order radiative rate is expected. The faster radiative rate reduces the ASE threshold as it increases the photon density at short times after the pulsed excitation, and therefore the product of the photon and carrier densities. Both the enhanced radiative rate and suppressed trapping increase the PL efficiency, explaining the observations above. Under negative bias, we do not observe an increase in PL or ASE because the reduction in trap density is offset by enhanced nonradiative rates caused by faster carrier extraction. Figure S16 illustrates how the reverse bias causes carriers to drift toward the electrodes at which their extraction is energetically favorable.

The above model also indicates that the modulation of PL/ASE is only related to the direction of bias voltage, not the incident direction of the pulsed laser. As expected, we observe that the PL/ASE is also enhanced (reduced) on the application of positive (negative) voltage when the pulsed laser is incident on the ETL side (Figure S17). As illustrated in Figure S18, we have conducted measurements on electrically insulating devices with blocking layers either directly adjacent to the perovskite layer or between the contacts and carrier transport layers. Our results show that while the former does not exhibit modulation of PL/ASE upon the application of an electric field, the latter does. This confirms that it is the electric field, not current, that is responsible for bias-modulated PL/ASE. We also note that the carrier transport layers seem to play a role in ion migration and recovery under an electric field, as previously reported in literature.[49] Further research into this mechanism is currently ongoing. Furthermore, the positive DC bias induced PL enhancement with slow transients in response to the external bias are observed both for $CsPbBr_3$ LED (low optical power excitation, Figure S19) and triple cation perovskite solar cells[50] (Figure S20). This further supports our model of ion migration and its effect on emission efficiency, and suggests that this PL enhancement due to ion migration can occur in multiple perovskite-based material compositions.

Our current work reveals that the ASE and PL performance of $CsPbBr_3$ can be significantly enhanced by a positive bias, even though the electrically injected carrier density is far too low to have such a major impact on light emission. Our data suggests that sweeping the mobile ions out from the bulk of the film significantly increases the radiative efficiency and optical gain. In terms of electrical pumping, intense current driven LEDs[17−20] adopt brief electrical pulses (ns to μs length), which are too short to redistribute the mobile ions. Therefore, driving such LEDs under simultaneous DC and pulsed electrical excitation may be helpful for realizing the electrical injection lasing.[15] Meanwhile, increasing the duty cycle of the pulsed electrical excitation could also be beneficial,[15] as the time for sweeping the ions away is increased and the time for their recovery is reduced.

We report a repeatable modulation of PL and ASE in $CsPbBr_3$ based LEDs triggered by switching a positive bias voltage on and off while maintaining a constant subthreshold optical excitation. The applied bias can reduce the ASE threshold by a factor of 3 when applying a positive bias voltage over 4 V. The response of the ASE and PL to a change in the applied bias is very slow, with transients on the order of several seconds. This implies that the ion motion is likely to underlie the effect. PLQY and TRPL measurements as a function of applied bias show that the bimolecular radiative rate is increased, and the first and second-order trap-associated decay is reduced by the application of a positive bias. This explains both the enhanced PL (better competition against nonradiative rates) and the enhanced ASE (faster photon emission leading to a larger product of the photon and charge carrier densities and therefore enhanced gain). This work establishes the importance of mobile ions for optical gain and demonstrates that significant improvement in gain performance can be achieved when ions are extracted from the volume of the material responsible for gain. This has implications for pumping schemes for electrically pumped lasing but should also be considered for optical gain materials and from a fundamental perovskite development perspective.

■ ASSOCIATED CONTENT

Supporting Information

The Supporting Information is available free of charge at https://pubs.acs.org/doi/10.1021/acs.nanolett.2c02944.

Additional details of materials and methods, calculation on electrically injected carrier density, additional figures including device engineering toward ASE, EL performance, EL and PL comparison, LED hysteresis, ASE threshold measurement under DC biases or CW optical biases, TRPL, band alignment, voltage-emission characteristics upon laser incident (PDF)

Additional video showing the electric-field-assisted modulation of ASE (MP4)

■ AUTHOR INFORMATION

Corresponding Authors

Yang Li − *Institute of Microstructure Technology, Karlsruhe Institute of Technology, 76344 Eggenstein-Leopoldshafen, Germany; Light Technology Institute, Karlsruhe Institute of*

https://doi.org/10.1021/acs.nanolett.2c02944
Nano Lett. XXXX, XXX, XXX−XXX

Technology, 76131 Karlsruhe, Germany; orcid.org/0000-0002-4894-679X; Email: yang.li2@kit.edu

Ulrich W. Paetzold − *Institute of Microstructure Technology, Karlsruhe Institute of Technology, 76344 Eggenstein-Leopoldshafen, Germany; Light Technology Institute, Karlsruhe Institute of Technology, 76131 Karlsruhe, Germany;* orcid.org/0000-0002-1557-8361; Email: ulrich.paetzold@kit.edu

Ian A. Howard − *Institute of Microstructure Technology, Karlsruhe Institute of Technology, 76344 Eggenstein-Leopoldshafen, Germany; Light Technology Institute, Karlsruhe Institute of Technology, 76131 Karlsruhe, Germany;* orcid.org/0000-0002-7327-7356; Email: ian.howard@kit.edu

Authors

Hang Hu − *Institute of Microstructure Technology, Karlsruhe Institute of Technology, 76344 Eggenstein-Leopoldshafen, Germany; Light Technology Institute, Karlsruhe Institute of Technology, 76131 Karlsruhe, Germany;* orcid.org/0000-0001-8141-8772

Ahmed Farag − *Institute of Microstructure Technology, Karlsruhe Institute of Technology, 76344 Eggenstein-Leopoldshafen, Germany; Light Technology Institute, Karlsruhe Institute of Technology, 76131 Karlsruhe, Germany*

Thomas Feeney − *Institute of Microstructure Technology, Karlsruhe Institute of Technology, 76344 Eggenstein-Leopoldshafen, Germany; Light Technology Institute, Karlsruhe Institute of Technology, 76131 Karlsruhe, Germany*

Isabel Allegro − *Light Technology Institute, Karlsruhe Institute of Technology, 76131 Karlsruhe, Germany;* orcid.org/0000-0001-9663-4910

Uli Lemmer − *Institute of Microstructure Technology, Karlsruhe Institute of Technology, 76344 Eggenstein-Leopoldshafen, Germany; Light Technology Institute, Karlsruhe Institute of Technology, 76131 Karlsruhe, Germany;* orcid.org/0000-0001-9892-329X

Complete contact information is available at: https://pubs.acs.org/10.1021/acs.nanolett.2c02944

Author Contributions

Y.L., U.W.P, and I.A.H. proposed the idea for this project. Y.L. fabricated the samples and conducted the optical characterization. I.A. assisted with optical characterization. H.H., and T.F. performed and optimized the ALD deposition process for Al_2O_3 thin films. A.F. performed and optimized the sputtering process for ITO thin films. All the authors contributed to the discussion and data analysis. Y.L., U.W.P., and I.A.H. wrote the manuscript with inputs from all the others. U.L., U.W.P., and I.A.H. supervised this project.

Notes

The authors declare no competing financial interest.

■ ACKNOWLEDGMENTS

The authors gratefully acknowledge funding from the DFG (PEROLAS, no. 409035484), the Karlsruhe School of Optics & Photonics (KSOP) financed by the Ministry of Science, Research and the Arts of Baden-Wuerttemberg as part of the sustainability financing of the projects of the Excellence Initiative II, the Karlsruhe Nano Micro Facility (KNMF), the Helmholtz Energy Materials Foundry (HEMF), and the Excellence Cluster "3D Matter Made to Order" (EXC-2082/1-390761711). The authors thank the Helmholtz Association MTET program (Materials and Technologies for the Energy Transition) − Topic 1 − Photovoltaics (38.01.05). H.H. would like to thank the financial support from the Chinese Scholarship Council (CSC, no. 201808420221).

■ REFERENCES

(1) Quan, L. N.; Rand, B. P.; Friend, R. H.; Mhaisalkar, S. G.; Lee, T.-W.; Sargent, E. H. Perovskites for Next-Generation Optical Sources. *Chem. Rev.* **2019**, *119*, 7444−7477.

(2) Lei, L.; Dong, Q.; Gundogdu, K.; So, F. Metal Halide Perovskites for Laser Applications. *Adv. Funct. Mater.* **2021**, *31*, 2010144.

(3) Gunnarsson, W. B.; Rand, B. P. Electrically driven lasing in metal halide perovskites: Challenges and outlook. *APL Materials* **2020**, *8*, 030902.

(4) Deschler, F.; Price, M.; Pathak, S.; Klintberg, L. E.; Jarausch, D.-D.; Higler, R.; Hüttner, S.; Leijtens, T.; Stranks, S. D.; Snaith, H. J.; Atatüre, M.; Phillips, R. T.; Friend, R. H. High Photoluminescence Efficiency and Optically Pumped Lasing in Solution-Processed Mixed Halide Perovskite Semiconductors. *J. Phys. Chem. Lett.* **2014**, *5*, 1421−1426.

(5) Sutherland, B. R.; Hoogland, S.; Adachi, M. M.; Wong, C. T. O.; Sargent, E. H. Conformal Organohalide Perovskites Enable Lasing on Spherical Resonators. *ACS Nano* **2014**, *8*, 10947−10952.

(6) Xing, G.; Mathews, N.; Lim, S. S.; Yantara, N.; Liu, X.; Sabba, D.; Grätzel, M.; Mhaisalkar, S.; Sum, T. C. Low-temperature solution-processed wavelength-tunable perovskites for lasing. *Nat. Mater.* **2014**, *13*, 476.

(7) Zhang, Q.; Ha, S. T.; Liu, X.; Sum, T. C.; Xiong, Q. Room-temperature near-infrared high-Q perovskite whispering-gallery planar nanolasers. *Nano Lett.* **2014**, *14*, 5995−6001.

(8) Cadelano, M.; Sarritzu, V.; Sestu, N.; Marongiu, D.; Chen, F.; Piras, R.; Corpino, R.; Carbonaro, C. M.; Quochi, F.; Saba, M.; Mura, A.; Bongiovanni, G. Can. Trihalide Lead Perovskites Support Continuous Wave Lasing? *Adv. Optical Mater.* **2015**, *3*, 1557−1564.

(9) Chen, S.; Roh, K.; Lee, J.; Chong, W. K.; Lu, Y.; Mathews, N.; Sum, T. C.; Nurmikko, A. A Photonic Crystal Laser from Solution Based Organo-Lead Iodide Perovskite Thin Films. *ACS Nano* **2016**, *10*, 3959−67.

(10) Whitworth, G. L.; Harwell, J. R.; Miller, D. N.; Hedley, G. J.; Zhang, W.; Snaith, H. J.; Turnbull, G. A.; Samuel, I. D. Nanoimprinted distributed feedback lasers of solution processed hybrid perovskites. *Opt. Express* **2016**, *24*, 23677−23684.

(11) Jia, Y. F.; Kerner, R. A.; Grede, A. J.; Rand, B. P.; Giebink, N. C. Continuous-wave lasing in an organic-inorganic lead halide perovskite semiconductor. *Nat. Photonics* **2017**, *11*, 784−788.

(12) Brenner, P.; Bar-On, O.; Jakoby, M.; Allegro, I.; Richards, B. S.; Paetzold, U. W.; Howard, I. A.; Scheuer, J.; Lemmer, U. Continuous wave amplified spontaneous emission in phase-stable lead halide perovskites. *Nat. Commun.* **2019**, *10*, 988.

(13) Roh, K.; Zhao, L.; Rand, B. P. Tuning Laser Threshold within the Large Optical Gain Bandwidth of Halide Perovskite Thin Films. *ACS Photonics* **2021**, *8*, 2548−2554.

(14) Qin, C.; Sandanayaka, A. S. D.; Zhao, C.; Matsushima, T.; Zhang, D.; Fujihara, T.; Adachi, C. Stable room-temperature continuous-wave lasing in quasi-2D perovskite films. *Nature* **2020**, *585*, 53−57.

(15) Kim, H.; Zhao, L.; Price, J. S.; Grede, A. J.; Roh, K.; Brigeman, A. N.; Lopez, M.; Rand, B. P.; Giebink, N. C. Hybrid perovskite light emitting diodes under intense electrical excitation. *Nat. Commun.* **2018**, *9*, 4893.

(16) Yuan, F.; Xi, J.; Dong, H.; Xi, K.; Zhang, W.; Ran, C.; Jiao, B.; Hou, X.; Jen, A. K.-Y.; Wu, Z. All-Inorganic Hetero-Structured Cesium Tin Halide Perovskite Light-Emitting Diodes With Current

Density Over 900 A cm^{-2} and Its Amplified Spontaneous Emission Behaviors. *Phys. Status Solidi RRL* **2018**, *12*, 1800090.
(17) Zou, C.; Liu, Y.; Ginger, D. S.; Lin, L. Y. Suppressing Efficiency Roll-Off at High Current Densities for Ultra-Bright Green Perovskite Light-Emitting Diodes. *ACS Nano* **2020**, *14*, 6076−6086.
(18) Cho, C.; Antrack, T.; Kroll, M.; An, Q.; Barschneider, T. R.; Fischer, A.; Meister, S.; Vaynzof, Y.; Leo, K. Electrical Pumping of Perovskite Diodes: Toward Stimulated Emission. *Adv. Sci.* **2021**, *8*, 2101663.
(19) Zhao, L.; Roh, K.; Kacmoli, S.; Al Kurdi, K.; Liu, X.; Barlow, S.; Marder, S. R.; Gmachl, C.; Rand, B. P. Nanosecond-Pulsed Perovskite Light-Emitting Diodes at High Current Density. *Adv. Mater.* **2021**, *33*, 2104867.
(20) Elkhouly, K.; Goldberg, I.; Annavarapu, N.; Gehlhaar, R.; Ke, T.-H.; Genoe, J.; Hofkens, J.; Heremans, P.; Qiu, W. Intense Electrical Pulsing of Perovskite Light Emitting Diodes under Cryogenic Conditions. *Adv. Optical Mater.* **2022**, *10*, 2200024.
(21) Yuan, F.; Wu, Z.; Dong, H.; Xia, B.; Xi, J.; Ning, S.; Ma, L.; Hou, X. Electric field-modulated amplified spontaneous emission in organo-lead halide perovskite $CH_3NH_3PbI_3$. *Appl. Phys. Lett.* **2015**, *107*, 261106.
(22) Yi, H. T.; Rangan, S.; Tang, B.; Frisbie, C. D.; Bartynski, R. A.; Gartstein, Y. N.; Podzorov, V. Electric-field effect on photoluminescence of lead-halide perovskites. *Mater. Today* **2019**, *28*, 31−39.
(23) Kim, H.; Roh, K.; Murphy, J. P.; Zhao, L.; Gunnarsson, W. B.; Longhi, E.; Barlow, S.; Marder, S. R.; Rand, B. P.; Giebink, N. C. Optically Pumped Lasing from Hybrid Perovskite Light-Emitting Diodes. *Adv. Optical Mater.* **2020**, *8*, 1901297.
(24) Gao, Y.; Li, X.; Liu, W.; Xing, X.; Long, H.; Wang, K.; Wang, B.; Lu, P. Highly Tunable Enhancement and Switching of Nonlinear Emission from All-Inorganic Lead Halide Perovskites via Electric Field. *Nano Lett.* **2021**, *21*, 10230−10237.
(25) Liu, P.; Gu, C.; Liao, Q. Electrically Switchable Amplified Spontaneous Emission from Lead Halide Perovskite Film. *ACS omega* **2021**, *6*, 34021−34026.
(26) Li, N.; Jia, Y.; Guo, Y.; Zhao, N. Ion Migration in Perovskite Light-Emitting Diodes: Mechanism, Characterizations, and Material and Device Engineering. *Adv. Mater.* **2022**, *34*, 2108102.
(27) Kamat, P. V.; Kuno, M. Halide Ion Migration in Perovskite Nanocrystals and Nanostructures. *Acc. Chem. Res.* **2021**, *54*, 520−531.
(28) Eames, C.; Frost, J. M.; Barnes, P. R. F.; O'Regan, B. C.; Walsh, A.; Islam, M. S. Ionic transport in hybrid lead iodide perovskite solar cells. *Nat. Commun.* **2015**, *6*, 7497.
(29) Zhang, T.; Chen, H.; Bai, Y.; Xiao, S.; Zhu, L.; Hu, C.; Xue, Q.; Yang, S. Understanding the relationship between ion migration and the anomalous hysteresis in high-efficiency perovskite solar cells: A fresh perspective from halide substitution. *Nano Energy* **2016**, *26*, 620−630.
(30) Xiao, Z.; Yuan, Y.; Shao, Y.; Wang, Q.; Dong, Q.; Bi, C.; Sharma, P.; Gruverman, A.; Huang, J. Giant switchable photovoltaic effect in organometal trihalide perovskite devices. *Nat. Mater.* **2015**, *14*, 193−198.
(31) Wang, H.; Chen, Z.; Hu, J.; Yu, H.; Kuang, C.; Qin, J.; Liu, X.; Lu, Y.; Fahlman, M.; Hou, L.; Liu, X. K.; Gao, F. Dynamic Redistribution of Mobile Ions in Perovskite Light-Emitting Diodes. *Adv. Funct. Mater.* **2021**, *31*, 2007596.
(32) Li, J.; Chen, Y.; Zhang, B.; Li, J.; Uddin, Z.; Jiang, X.; Wang, X.; Hong, J.; Yuan, Y.; Stathatos, E.; Xiao, H.; Pan, A.; Liu, Y.; Yang, B. Non-Traditional Positively-Biased Narrow-Band Perovskite Single-Crystal Photodetectors Enabled by Interfacial Engineering. *Adv. Optical Mater.* **2022**, *10*, 2102225.
(33) Cai, J.; Zhao, T.; Chen, M.; Su, J.; Shen, X.; Liu, Y.; Cao, D. Ion Migration in the All-Inorganic Perovskite $CsPbBr_3$ and Its Impacts on Photodetection. *J. Phys. Chem. C* **2022**, *126*, 10007−10013.
(34) Dong, Q.; Mendes, J.; Lei, L.; Seyitliyev, D.; Zhu, L.; He, S.; Gundogdu, K.; So, F. Understanding the Role of Ion Migration in the Operation of Perovskite Light-Emitting Diodes by Transient Measurements. *ACS Appl. Mater. Interfaces* **2020**, *12*, 48845−48853.
(35) Zhang, T.; Cheung, S. H.; Meng, X.; Zhu, L.; Bai, Y.; Ho, C. H. Y.; Xiao, S.; Xue, Q.; So, S. K.; Yang, S. Pinning Down the Anomalous Light Soaking Effect toward High-Performance and Fast-Response Perovskite Solar Cells: The Ion-Migration-Induced Charge Accumulation. *J. Phys. Chem. Lett.* **2017**, *8*, 5069−5076.
(36) Chmeliov, J.; Elkhouly, K.; Gegevičius, R.; Jonušis, L.; Devižis, A.; Gelžinis, A.; Franckevičius, M.; Goldberg, I.; Hofkens, J.; Heremans, P.; Qiu, W.; Gulbinas, V. Ion Motion Determines Multiphase Performance Dynamics of Perovskite LEDs. *Adv. Optical Mater.* **2021**, *9*, 2101560.
(37) Li, Y.; Allegro, I.; Kaiser, M.; Malla, A. J.; Richards, B. S.; Lemmer, U.; Paetzold, U. W.; Howard, I. A. Exciton versus free carrier emission: Implications for photoluminescence efficiency and amplified spontaneous emission thresholds in quasi-2D and 3D perovskites. *Mater. Today* **2021**, *49*, 35−47.
(38) Li, Y.; Roger, J.; Allegro, I.; Fischer, J. C.; Jin, Q.; Lemmer, U.; Howard, I. A.; Paetzold, U. W. Lasing from Laminated Quasi-2D/3D Perovskite Planar Heterostructures. *Adv. Funct. Mater.* **2022**, *32*, 2200772.
(39) Richter, J. M.; Abdi-Jalebi, M.; Sadhanala, A.; Tabachnyk, M.; Rivett, J. P. H.; Pazos-Outón, L. M.; Gödel, K. C.; Price, M.; Deschler, F.; Friend, R. H. Enhancing photoluminescence yields in lead halide perovskites by photon recycling and light out-coupling. *Nat. Commun.* **2016**, *7*, 13941.
(40) Brenes, R.; Guo, D.; Osherov, A.; Noel, N. K.; Eames, C.; Hutter, E. M.; Pathak, S. K.; Niroui, F.; Friend, R. H.; Islam, M. S.; Snaith, H. J.; Bulović, V.; Savenije, T. J.; Stranks, S. D. Metal Halide Perovskite Polycrystalline Films Exhibiting Properties of Single Crystals. *Joule* **2017**, *1*, 155−167.
(41) Péan, E. V.; Dimitrov, S.; De Castro, C. S.; Davies, M. L. Interpreting time-resolved photoluminescence of perovskite materials. *Phys. Chem. Chem. Phys.* **2020**, *22*, 28345−28358.
(42) Simbula, A.; Pau, R.; Liu, F.; Wu, L.; Lai, S.; Geddo-Lehmann, A.; Filippetti, A.; Loi, M. A.; Marongiu, D.; Quochi, F.; Saba, M.; Mura, A.; Bongiovanni, G. Direct measurement of radiative decay rates in metal halide perovskites. *Energy Environ. Sci.* **2022**, *15*, 1211−1221.
(43) Hutter, E. M.; Savenije, T. J. Thermally Activated Second-Order Recombination Hints toward Indirect Recombination in Fully Inorganic $CsPbI_3$ Perovskites. *ACS Energy Lett.* **2018**, *3*, 2068−2069.
(44) Kiligaridis, A.; Frantsuzov, P. A.; Yangui, A.; Seth, S.; Li, J.; An, Q.; Vaynzof, Y.; Scheblykin, I. G. Are Shockley-Read-Hall and ABC models valid for lead halide perovskites? *Nat. Commun.* **2021**, *12*, 3329.
(45) Allegro, I.; Li, Y.; Richards, B. S.; Paetzold, U. W.; Lemmer, U.; Howard, I. A. Bimolecular and Auger Recombination in Phase-Stable Perovskite Thin Films from Cryogenic to Room Temperature and Their Effect on the Amplified Spontaneous Emission Threshold. *J. Phys. Chem. Lett.* **2021**, *12*, 2293−2298.
(46) Huang, C.-Y.; Wu, C.-C.; Wu, C.-L.; Lin, C.-W. $CsPbBr_3$ Perovskite Powder, a Robust and Mass-Producible Single-Source Precursor: Synthesis, Characterization, and Optoelectronic Applications. *ACS omega* **2019**, *4*, 8081−8086.
(47) Schwenzer, J. A.; Rakocevic, L.; Gehlhaar, R.; Abzieher, T.; Gharibzadeh, S.; Moghadamzadeh, S.; Quintilla, A.; Richards, B. S.; Lemmer, U.; Paetzold, U. W. Temperature Variation-Induced Performance Decline of Perovskite Solar Cells. *ACS Appl. Mater. Interfaces* **2018**, *10*, 16390−16399.
(48) Herz, L. M. Charge-Carrier Mobilities in Metal Halide Perovskites: Fundamental Mechanisms and Limits. *ACS Energy Lett.* **2017**, *2*, 1539−1548.
(49) Teng, P.; Reichert, S.; Xu, W.; Yang, S.-C.; Fu, F.; Zou, Y.; Yin, C.; Bao, C.; Karlsson, M.; Liu, X.; Qin, J.; Yu, T.; Tress, W.; Yang, Y.; Sun, B.; Deibel, C.; Gao, F. Degradation and self-repairing in perovskite light-emitting diodes. *Matter* **2021**, *4*, 3710−3724.
(50) Ruiz-Preciado, M. A.; Gota, F.; Fassl, P.; Hossain, I. M.; Singh, R.; Laufer, F.; Schackmar, F.; Feeney, T.; Farag, A.; Allegro, I.; Hu, H.; Gharibzadeh, S.; Nejand, B. A.; Gevaerts, V. S.; Simor, M.; Bolt, P. J.; Paetzold, U. W. Monolithic Two-Terminal Perovskite/CIS

https://doi.org/10.1021/acs.nanolett.2c02944
Nano Lett. XXXX, XXX, XXX−XXX

Tandem Solar Cells with Efficiency Approaching 25%. *ACS Energy Lett.* **2022**, *7*, 2273−2281.

https://doi.org/10.1021/acs.nanolett.2c02944
Nano Lett. XXXX, XXX, XXX−XXX